MeshCone: Second-Order Cone Programming for Geometrically-Constrained Mesh Enhancement

Alexander Valverde

University of California, Santa Cruz

Abstract

Modern mesh generation pipelines—whether learning-based or classical—often produce outputs requiring post-processing to achieve production-quality geometry. This work introduces MeshCone, a convex optimization framework for guided mesh refinement that leverages reference geometry to correct deformed or degraded meshes. We formulate the problem as a second-order cone program where vertex positions are optimized to align with target geometry while enforcing smoothness through convex edge-length regularization. MeshCone performs geometry-aware optimization that preserves fine details while correcting structural defects. We demonstrate robust performance across 56 diverse object categories from ShapeNet and ThreeDScans, achieving superior refinement quality compared to Laplacian smoothing and unoptimized baselines while maintaining sub-second inference times. MeshCone is particularly suited for applications where reference geometry is available, such as mesh-from-template workflows, scan-to-CAD alignment, and quality assurance in asset production pipelines.

1 Introduction

The field of computer graphics has been deeply engaged with mesh generation since the introduction of the Marching Cubes algorithm [35] nearly four decades ago. Over the years, diverse techniques have emerged—from classical methods based on Signed Distance Fields (SDFs) and Radial Basis Functions (RBFs) to modern learning-based approaches using neural networks

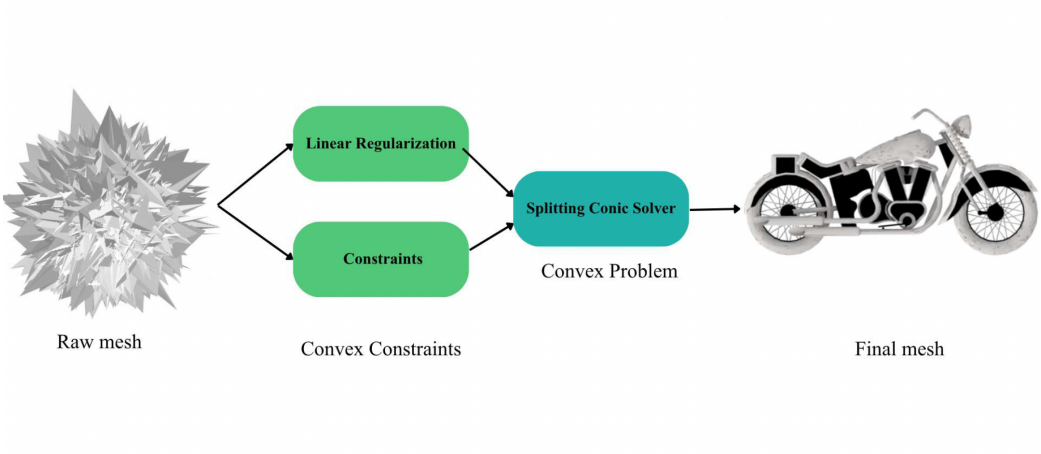

Figure 1: Overview of the MeshCone framework. Starting from a shapeless input mesh, we formulate the refinement as a second-order cone program with linear regularization and smoothness constraints, which is solved using the Splitting Conic Solver to produce a refined mesh.

and autoregressive architectures. Yet regardless of the generation method, a persistent challenge remains: *how can we efficiently refine imperfect meshes toward high-quality target geometry with mathematical guarantees?*

Modern mesh generation pipelines—whether classical or learning-based—frequently produce outputs that require post-processing before deployment. Generated meshes may exhibit noise, geometric distortions, or deviation from intended shapes. While learning-based refinement methods can address these issues, they require extensive training data, lack interpretability, and provide no formal guarantees about solution quality or convergence. This motivates the need for principled refinement approaches that can leverage available reference geometry to correct mesh defects reliably and predictably.

Convex optimization has long been a cornerstone of fields such as finance, engineering, and economics, offering a principled framework that guarantees globally optimal solutions under well-defined constraints. Its efficiency, robustness, and optimality make it desirable for applications where stability and reproducibility are essential. Within computer graphics, optimization techniques are common in mesh processing tasks—such as parameterization, deformation, and smoothing—yet few works investigate whether convex formulations can serve as effective *guided refinement* methods that leverage target geometry to achieve provably optimal corrections.

This work introduces **MeshCone**, a conic optimization framework for geometry-guided mesh refinement. Given a source mesh and reference target geometry, MeshCone formulates refinement as a second-order cone program (SOCP) that optimizes vertex positions to align with the target while enforcing smoothness via convex edge-length constraints and Tikhonov regulariza-

tion. By employing the Splitting Conic Solver (SCS), we obtain solutions with provable global optimality, guaranteed convergence at rate $O(1/k)$, and Lipschitz stability under perturbations—properties unavailable in heuristic or neural approaches.

Unlike blind smoothing methods such as Laplacian filtering that uniformly regularize without geometric awareness, MeshCone performs target-aware optimization that preserves fine details present in the reference while correcting structural defects in the source mesh. This makes our approach particularly suited for workflows where reference geometry is available, including:

Our contributions are as follows:

- **Formulation:** We present the first formulation of mesh processing as a second-order cone program with provable global optimality guarantees, establishing a principled optimization baseline for the task.
- **Theoretical analysis:** We establish convergence rate $O(1/k)$, Lipschitz stability bounds, and sparsity properties $\mathcal{O}(n)$ that enable efficient large-scale optimization, with explicit connections to geometric mesh quality criteria.
- **Baseline establishment:** We provide a deterministic, geometry-aware baseline with mathematical guarantees against which future optimization-based and hybrid methods can be compared, identifying both capabilities and limitations of pure convex approaches.

2 Related Work

2.1 Surface Reconstruction Methods

Classical surface reconstruction has long been a central topic in computer graphics, providing the foundation for obtaining polygonal meshes from raw geometric data such as point clouds, volumetric grids, or 2D imagery. Early approaches focused on *isosurface extraction*, where methods like *Marching Cubes* [36] enabled the generation of polygonal surfaces from discrete scalar fields by linearly interpolating intersections along voxel edges. Subsequent advances introduced *volumetric techniques* such as Signed Distance Fields (SDFs) and Truncated Signed Distance Fields (TSDFs), which represent objects as continuous implicit functions over 3D space. [17] pioneered the use of cumulative signed distance functions for reconstructing models from

range images, a formulation later adopted in modern real-time 3D scanning and SLAM systems.

Beyond discrete isosurfaces, implicit formulations have become an important class of reconstruction methods. [62] introduced a level-set approach based on partial differential equations (PDEs), evolving an implicit surface toward the observed data by solving time-dependent variational flows. [29] later proposed the *Poisson Surface Reconstruction*, which formulates surface fitting as a global spatial Poisson problem over oriented points.

2.2 Mesh Generation

Several papers generate meshes by first learning implicit representations and then extracting surfaces. DMTet [47] uses a hybrid representation combining deep marching tetrahedra with differentiable rendering. FlexiCubes [48] extends this with a flexible isosurface representation that adaptively adjusts to local geometric complexity. NeuralMarchingCubes [15] learns to predict signed distance fields that can be converted to meshes via differentiable marching cubes. TetWeave [5] introduces on-the-fly Delaunay tetrahedral grids for isosurface extraction, enabling gradient-based mesh optimization directly from implicit functions.

Autoregressive models have been widely used recently to recreate meshes as structured sequences of vertices, faces, or learned tokens. Recent examples include PolyGen [39], MeshGPT [52], MeshAnything and MeshAnything V2 [13, 14], TreeMeshGPT [34], MeshArt [60], MeshMamba [58], and the autoregressive auto-encoder ArAE [55].

Earlier deep-learning methods generate or refine meshes through differentiable deformation, atlas parameterization, or neural rendering. Techniques such as AtlasNet [24], Pixel2Mesh and Pixel2Mesh++ [57, 59], Mesh R-CNN [23], Neural 3D Mesh Renderer [28], DIB-R [12], GEOMetrics [53], and GET3D [22] remain influential baselines that established neural architectures for mesh deformation and reconstruction.

2.3 Mesh Refinement

Three-dimensional mesh refinement presents important challenges due to geometric complexity and the need to maintain element quality during subdivision. Foundational error estimation frameworks [3] and longest-edge bisection algorithms for tetrahedral meshes [43, 44] established the theoretical basis for adaptive 3D refinement. Practical refinement strategies include octree-based approaches with transition elements for hexahedral meshes [46, 61], quality preservation through optimization-based smoothing and topological

operations [20, 31, 50], and anisotropic adaptation using Riemannian metric tensors [1, 21, 37]. Scalable parallel implementations include forest-of-octrees algorithms [10, 54] and block-structured adaptation frameworks [38]. In geometry processing, remeshing and optimization frameworks such as directional field-guided parameterization and curvature-aware remeshing [26, 27] have shown high-quality surface refinement.

2.4 Convex Optimization in 3D

Convex optimization techniques have been increasingly adopted in recent years for 3D reconstruction and scene representation tasks. [18] introduced *CVXNet*, a framework that reconstructs 3D objects from input images by decomposing them into a collection of convex primitives. Each primitive is represented as a convex hull, allowing the network to generate a polygonal mesh composed of multiple convex polytopes with well-defined geometric boundaries. Similarly, [49] proposed a convex optimization-based approach for texture mapping in large-scale 3D scenes.

Building upon these developments, convex representations have also gained attention in novel view synthesis. [25] introduced *3D Convex Splatting (3DCS)*, which marks a conceptual shift from the Gaussian primitives employed in *3D Gaussian Splatting (3DGS)* [30]. Instead of modeling scenes as sets of anisotropic Gaussians, 3DCS uses smooth convex primitives inspired by the theoretical foundations of CVXNet [18].

3 Method

In this work, we introduce a convex optimization framework for mesh adjustment via structural correction. The proposed method builds upon the theoretical foundations of convex programming and leverages the *Splitting Conic Solver (SCS)* to efficiently transform an unrefined or noisy mesh into a geometrically consistent and well-defined surface. We conduct a comprehensive analysis of convex optimization principles to justify the use of this solver, emphasizing its convergence guarantees, scalability, and suitability for large-scale geometric problems. Furthermore, we define a set of convex constraints that enforce local smoothness and global consistency, guiding the refined mesh to approximate the target geometry as closely as possible.

3.1 3D Mesh Overview

A three-dimensional mesh can be formally defined as

$$M = (V, E, F),$$

where $V \in \mathbb{R}^{n\times 3}$ denotes the set of n vertices representing the spatial coordinates of the surface, and F is the set of polygonal faces that connect these vertices to form the surface topology. The set of edges $E \subseteq V \times V$ corresponds to the pairwise connections between adjacent vertices. These edges play a fundamental role in determining the local geometric structure of the mesh and are often used to enforce smoothness, apply deformation constraints, or ensure that the resulting mesh satisfies the properties of a well-defined and manifold surface.

A well-defined mesh must satisfy several fundamental conditions to ensure both geometric fidelity and numerical stability. First, the *accuracy of boundary representation* guarantees that the mesh closely conforms to the underlying geometry, preserving sharp features and surface contours [2]. Second, *element quality* measures the regularity and shape of faces or tetrahedra, preventing degenerate or ill-conditioned elements that may compromise numerical solvers [51]. Third, *density control* regulates the spatial distribution of vertices, ensuring adequate sampling of complex regions while maintaining computational efficiency [56]. Finally, *connectivity consistency* enforces a continuous and manifold topology without gaps, overlaps, or non-manifold edges, maintaining the structural integrity required for finite element analysis and geometric processing [16]. Collectively, these conditions define the quality criteria that any robust mesh must satisfy.

Given these conditions, it is essential to formulate the optimization problem in a manner that preserves these mesh properties throughout the refinement process. The proposed convex formulation aims to maintain boundary accuracy, element regularity, density consistency, and topological connectivity, ensuring that the resulting mesh remains both geometrically faithful and numerically stable.

3.2 Convex Optimization

Convex optimization is a subfield of mathematical optimization concerned with finding the optimal solution to a problem formulated under convexity constraints. This area has gained significant attention across various disciplines and remains one of the most extensively explored optimization frameworks, particularly since the publication of [9], where the authors established and proved fundamental concepts of convex analysis.

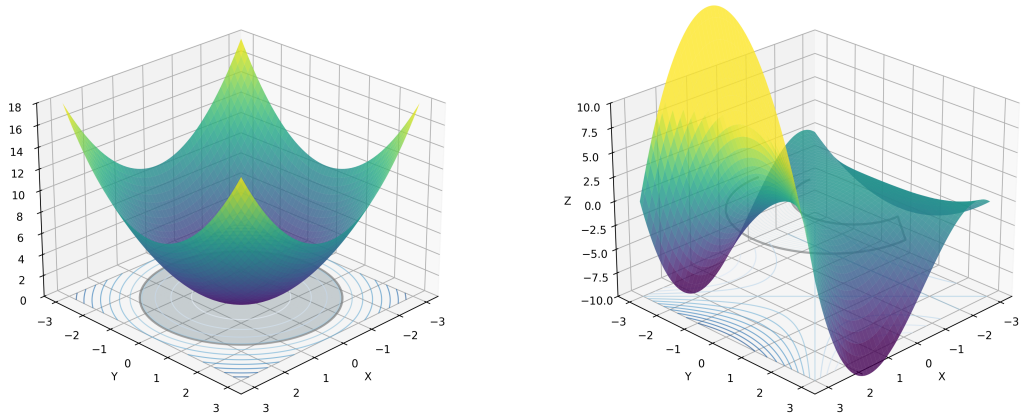

Figure 2: Comparison of optimization landscapes: (left) a convex objective function with convex constraints showing a single global minimum, (right) a nonconvex saddle function with nonconvex constraints exhibiting multiple local minimums.

It is grounded in the study of convex sets and convex functions. A convex set provides the geometric foundation for defining feasible regions, while convex functions, defined over such sets, ensure that every local minimum is also a global minimum. These properties make convex optimization both theoretically elegant and computationally tractable. We can define convex sets as:

A set $C \subseteq \mathbb{R}^n$ is said to be *convex* if, for any two points $x_1, x_2 \in C$ and any scalar $\theta \in [0, 1]$, the following condition holds:

$$\theta x_1 + (1 - \theta)x_2 \in C. \tag{1}$$

This definition implies that the line segment connecting any two points in C lies entirely within C.

With respect the functions, we need to use convex sets to define them because $f : \mathbb{R}^n \to \mathbb{R}$ is *convex* if its domain is a convex set and for all $x_1, x_2 \in \text{dom}(f)$ and any $\theta \in [0, 1]$, it satisfies

$$f(\theta x_1 + (1 - \theta)x_2) \leq \theta f(x_1) + (1 - \theta)f(x_2). \tag{2}$$

Geometrically, this means that the line segment between any two points on the graph of f lies above (or on) the graph itself.

A convex optimization problem can be formulated by defining an objective function together with a set of convex constraints that satisfy the properties of convexity. A problem is convex if it can be written as the maximization of a concave objective over a convex feasible set:

$$\max_{x \in \mathbb{R}^d} \phi(x) \quad \text{s.t.} \quad g_i(x) \leq 0 \ (i = 1, \ldots, m), \ h_j(x) = 0 \ (j = 1, \ldots, p),$$

where each g_i is convex and each h_j is affine, and ϕ is concave. Equivalently, one may minimize a convex function $f(x) = -\phi(x)$ under the same constraints.

3.2.1 Conic Solvers

In the field of convex optimization, several solvers are designed to handle specific classes of convex programs such as linear, quadratic, or exponential programs [33]. Depending on the structure and formulation of a given problem, an appropriate solver is selected to efficiently compute the optimal solution. Conic solvers, in particular, express optimization problems in conic form—where the feasible region is defined by constraints requiring variables to lie within a convex cone.

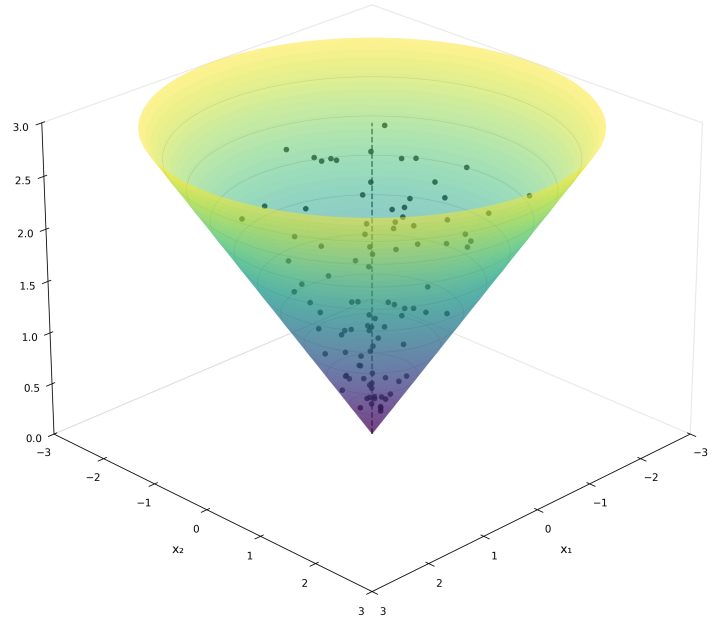

Figure 3: Second-Order Cone showing the constraint $\|\mathbf{x}\| \leq t$. The cone surface represents the feasible area boundary, with black points indicating valid solutions satisfying the constraint. For this example, t has a maximum value of 3

These solvers aim to find the minimum or maximum of an objective function subject to linear and conic constraints. Among the most common types of convex programs are linear programs (LPs), second-order cone programs

(SOCPs), and semidefinite programs (SDPs), each corresponding to a distinct class of convex cones and optimization properties.

For this specific scenario, the Splitting Conic Solver (SCS) is the one that fits better with our problem because it has a quadratic formulation. This is a numerical optimization method for solving large-scale convex quadratic cone problems. It is designed to solve large problems with thousands of constraints and variables in the following way:

$$\begin{array}{lll} \underset{x,\,s}{\text{minimize}} & \frac{1}{2}x^\top Px + c^\top x & \underset{y}{\text{maximize}} \quad -b^T y \\ \text{subject to} & Ax + s = b, & \text{subject to} \quad -A^T y + r = c, \\ & s \in \mathcal{K}. & (r, y) \in \{0\}^n \times \mathcal{K}^*. \end{array} \tag{3}$$

The conic optimization problem is defined over the following variables:

- $x \in \mathbb{R}^n$: primal variable,
- $y \in \mathbb{R}^m$: dual variable,
- $s \in \mathbb{R}^m$: primal slack variable.
- $r \in \mathbb{R}^m$: dual residual variable.

The problem is parameterized by the following data:

- $A \in \mathbb{R}^{m \times n}$: sparse data matrix,
- $P \in \mathbb{S}^n_+$: sparse, symmetric positive semidefinite matrix,
- $c \in \mathbb{R}^n$: dense primal cost vector,
- $b \in \mathbb{R}^m$: dense dual cost vector,
- $\mathcal{K} \subseteq \mathbb{R}^m$: nonempty, closed, convex cone,

The solver attempts to satisfy the optimality conditions to the desired accuracy, or provide a certificate of primal or dual infeasibility to the respective tolerance [41]. These optimizers work via the Alternating Direction Method of Multipliers (ADMM), an algorithm that solves large-scale convex problems by decomposing them into smaller, manageable subproblems [8]. This approach alternates between updating the primal variables x and the dual variables y (Lagrange multipliers). This alternating scheme allows the algorithm to exploit problem structure and work efficiently with sparse matrices, making the solution process significantly faster.

3.3 Mathematical Formulation

Given a target mesh to approximate, we begin with a partially deformed version that serves as our starting point for optimization. Let the deformed mesh be:

$$M_{\text{deformed}} = (V, F, E),$$

where $V = \{1, \ldots, n\}$ is the set of vertices, F the set of faces, and $E \subseteq V \times V$ the set of edges such that two vertices $i, j \in V$ are connected if they belong to a common face $f \in F$. Let $X \in \mathbb{R}^{n\times 3}$ be the matrix of vertex coordinates, where each row $X_i \in \mathbb{R}^3$ represents the 3D position of vertex i. The variable X is the decision variable of the optimization, representing the updated vertex positions.

From the deformed faces we extract the set of unique undirected edges $\mathcal{E} = \{(i_k, j_k)\}_{k=1}^{m} \subseteq V \times V$. Then, we sample N points from the target mesh surface and define their centroid $\mu \in \mathbb{R}^{1\times 3}$ by

$$\mu \;=\; \frac{1}{N}\sum_{\ell=1}^{N} p_\ell.$$

As a reference geometry for Tikhonov regularization, we use

$$\widehat{X} \;=\; \begin{cases} X_{\text{tgt}} & \text{if } \#V_{\text{tgt}} = \#V_{\text{deformed}}, \\ X_{\text{deformed}} & \text{otherwise,} \end{cases}$$

so that the regularizer is well-defined regardless of target topology.

We encourage coarse alignment to the target distribution via the centroid and penalize deviations from the reference geometry:

$$\min_{X\in\mathbb{R}^{n\times 3}} \|X - \mathbf{1}\mu\|_F^2 + \lambda \|X - \widehat{X}\|_F^2$$

where the first term enforces alignment of the optimized vertices with the target centroid, and the second term acts as a Tikhonov regularization that penalizes large deviations from the reference geometry. Here, $\lambda > 0$ controls the relative weight between alignment and regularization, and $\mathbf{1} \in \mathbb{R}^{n\times 1}$ denotes the all-ones vector.

3.3.1 Constraints

We define the constraint of this problem in the following way:

$$\|X_i - X_j\|_2 \leq \delta, \quad \forall (i,j) \in E,$$

where (i,j) denotes a pair of vertices connected by an edge in the mesh. Each $X_i, X_j \in \mathbb{R}^3$ represents the 3D coordinates of vertices i and j, respectively.

This ℓ_2-norm constraint ensures that the optimization process seeks a solution that minimizes the variation between connected vertices, effectively keeping edge lengths within a bounded range. Consequently, the optimized mesh remains geometrically consistent with the original structure while allowing controlled deformations toward the target shape.

Complete Optimization Problem

We define the convex optimization problem as

$$\begin{aligned} \min_{X \in \mathbb{R}^{n\times 3}} \quad & \underbrace{\|X - \mu \mathbf{1}^\top\|_F^2}_{\text{centroid alignment}} + \lambda \underbrace{\|X - X_{\text{ref}}\|_F^2}_{\text{regularization}} \\ \text{s.t.} \quad & \|X_i - X_j\|_2 \leq \delta, \quad \forall (i,j) \in E, \end{aligned}$$

where:

- $X \in \mathbb{R}^{n\times 3}$ is the decision variable collecting the vertex positions,
- $\mu = \frac{1}{m}\sum_{k=1}^{m} p_k \in \mathbb{R}^3$ is the centroid of the sampled target points,
- $X_{\text{ref}} = X_{\text{tgt}}$ if the target mesh has the same topology as the deformed mesh, otherwise $X_{\text{ref}} = X_{\text{deformed}}$,
- $\lambda > 0$ is the regularization weight, and
- $\delta > 0$ is a geometric smoothness threshold controlling the maximum allowed edge deformation.

4 Experiments

The implementation was developed using the PyTorch3D and CVXPY libraries. To thoroughly test our method's refinement capabilities, we create challenging test inputs by deforming a sphere toward target meshes from ShapeNet, stopping early to create heavily distorted, nearly shapeless meshes. This setup shows the limits of our approach: if MeshCone can successfully refine these badly inputs, it should handle less extreme cases

from real mesh generation methods. These partially deformed meshes represent the worst-case outputs that might come from incomplete optimization processes, generative model failures, or heavily corrupted 3D scans.

The approach is specifically evaluated on 53 meshes from the ShapeNet dataset [11], with each mesh representing a distinct object category. This diverse evaluation set spans the full range of ShapeNet taxonomy, including vehicles, furniture, electronics, kitchenware, and many other categories. This setup allows us to assess whether the optimization process can generalize across vastly different structures. In addition, we tested our solution against the classical Laplacian smoothing on three meshes generated from the work of [5], which are highly detailed and contain thousands of faces and vertices, making them ideal for a real-world test [32]. We sampled 10000 points from these representations to obtain the respective centroids used for alignment between the deformed vertices and the ground truth mesh.

For consistency and generalization, the same hyperparameters were used across all experiments. Specifically, we employed the SCS solver from CVXPY. We set $\lambda = 0.01$ and $\delta = 0.5$ for the regularization and smoothness constraints, respectively. The maximum number of iterations was fixed to 1000, and the solver tolerance ϵ was set to 1×10^{-5} with warm start enabled.

We created the initial mesh to have the same size as the target meshes in order to ensure consistency during the optimization process and to make it compatible with the SCS solver.

5 Results

The resulting meshes showed important properties maintained with respect the ground truth representations. Our 3D shapes showed connectivity, accurate boundary, proper density and good element quality. As can be seen in the qualitative examples our meshes maintain the same shape as the original ones and can be generated in a very short period of time, even less than a second in most of them. All results are presented with normalized meshes in a unit sphere.

As shown in Table 1, our full set of 53 meshes were processed in a total of 84 s, with an average runtime of approximately 1.22 s per mesh. This runtime accounts for the entire pipeline, from the misshapen input mesh to its optimized and refined version. We observed that more complex shapes can take over 5 s in certain cases, particularly when the surface contains numerous edges and irregularities that require higher solver precision. Furthermore, reducing the solver tolerance ϵ generally increases computation time, as the optimization requires more iterations to converge.

It is also worth noting that although we set the maximum number of iterations to 1000, the solver typically required only about 25 iterations to reach a primal residual smaller than ϵ, indicating fast convergence of our formulation. The success rate means that the convex solver achieved an optimal solution for the entire 53 meshes, what confirms the generalization of this method to different geometric figures.

Table 1: Solver statistics for ConvMesh optimization across 53 ShapeNet meshes.

	Avg. time (s)	Avg. iters	Success rate
Convex refinement	1.22	25	100%

Table 2 summarizes the average geometric evaluation metrics obtained across all reconstructed meshes. We selected Chamfer Distance (CD) and Earth Mover's Distance (EMD) to quantify geometric discrepancies between the predicted and reference surfaces, where lower values indicate better alignment and reconstruction fidelity.

To establish the value of our optimization framework, we compare against unoptimized meshes generated by two classical methods: Marching Cubes (MC) produces meshes from volumetric data, while Poisson Reconstruction (PR) generates surfaces from oriented point clouds. Both methods create initial meshes without subsequent refinement, representing the "No Optimization" baseline. Our method demonstrates substantial improvements across all metrics. Notably, MeshCone achieves a CD approximately 7.5× better than unoptimized Poisson Reconstruction and 1.3× better than unoptimized Marching Cubes, demonstrating that our optimization-based refinement significantly improves mesh quality regardless of the initial generation method.

Table 2: Average geometric evaluation metrics across all methods. Sampled 5000 points for evaluation across 53 meshes.

Method	**CD ↓**	**EMD ↓**	**HD ↓**	**NC ↑**	**CE ↓**
No Optimization (MC)	0.0038	0.125	0.311	0.686	0.062
No Optimization (PR)	0.0226	0.221	0.594	0.519	0.065
MeshCone (Ours)	**0.003**	**0.081**	**0.036**	**0.917**	**0.038**

To assess surface orientation preservation and fine-scale geometric fidelity, we computed Normal Consistency (NC), Hausdorff Distance (HD) and Curvature Error (CE) metrics. The HD is significantly lower than both baselines,

indicating better worst-case geometric accuracy. Most importantly, NC substantially outperforms both Marching Cubes and Poisson Reconstruction, demonstrating superior preservation of surface orientations.

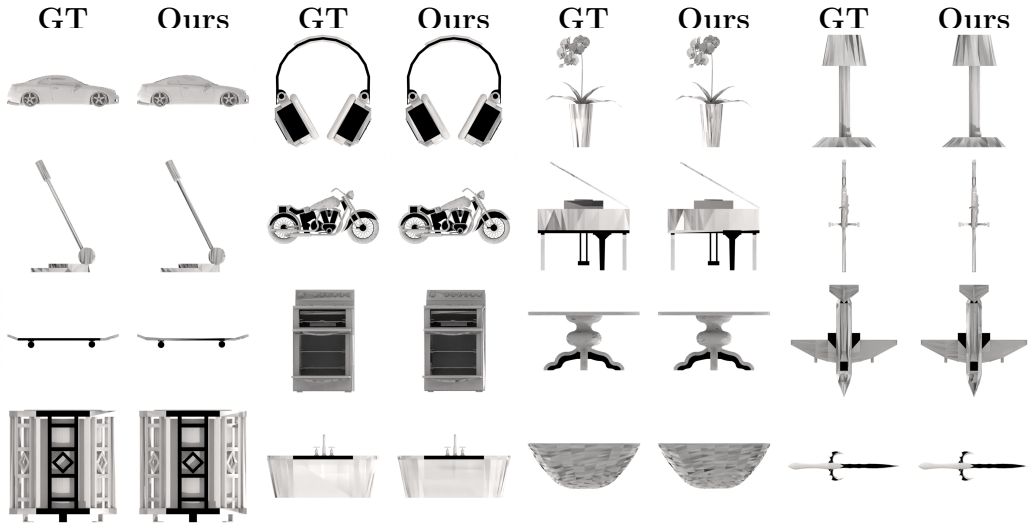

Figure 4: Qualitative results on 16 meshes from ShapeNetv2

As shown in Fig. 4, our qualitative evaluation demonstrates that the refined meshes exhibit high perceptual and geometric consistency with the ground-truth references. Complex structures, such as the intricate components of the motorcycle, are accurately recovered with minimal topological artifacts, while simpler geometries like the bowls and the sword are faithfully preserved. Furthermore, the proposed convex optimization framework effectively captures fine-scale details, as evidenced in the oven and kitchen reconstructions, where even small elements such as control buttons are well delineated. These results highlight the ability of our method to generalize across varying levels of structural complexity while maintaining high reconstruction fidelity.

Table 3: Comparison between raw TetWeave meshes and refined meshes after convex optimization

Representation	Metric	TetWeave	MeshCone
Beethoven	AR ↓	2.022	**1.862**
	EMD ↓	0.092	**0.091**
	HD ↓	0.165	**0.160**
Actaeon	AR ↓	1.696	**1.161**
	EMD ↓	0.0674	**0.0670**
	HD ↓	0.095	**0.092**
Goat	AR ↓	2.488	**1.935**
	EMD ↓	0.090	**0.086**
	HD ↓	0.165	**0.147**

In 3 we employed MeshCone to refined some meshes developed using the TetWeave paper [5]. Across the three selected models, MeshCone consistently outperform the raw TetWeave meshes in every metric. The average reconstruction error (AR) shows the most significant improvements, with reductions of 7.9% for Beethoven, 31.5% for Actaeon, and 22.2% for Goat, indicating that this process enhances the overall surface accuracy. EMD improvements are smaller but systematic, reflecting a tighter global alignment between the reconstructed and reference point distributions. HD values also decrease across all bodies, confirming that MeshCone effectively removes local outliers and geometric inconsistencies that remain in the TetWeave outputs. It is important to mention that the total optimization time is approximately 20 seconds per mesh, which makes this refinement practical to apply after mesh generation in highly-detailed figures, as it does not significantly affect the overall runtime of these pipelines, which typically range from 5 to 10 minutes per figure.

Figure 5: Quality comparison on three meshes: Ground Truth (left), TetWeave (middle left), Laplacian-smoothed TetWeave (middle right), and MeshCone (right).

Convex optimization provides the mathematical foundation for precise mesh refinement, guaranteeing global solutions that preserve geometric integrity—unlike Laplacian smoothing which destroys essential details through over-smoothing. Our framework demonstrates that convex solvers with linear constraints achieve optimal shape preservation and detail retention, offering stable, interpretable alternatives to complex non-convex approaches.

6 Ablations

We analyze the sensitivity of MeshCone to its regularization weight λ and edge constraint threshold δ. Table 4 shows results across three metrics: Hausdorff Distance (HD), Normal Consistency (NC), and total time (s). The default configuration ($\lambda = 0.01$, $\delta = 0.5$) achieves optimal balance across all criteria.

As shown in Table 4, the regularization weight λ demonstrates quality improvement, though the differences between these values are primarily related to execution time. Increasing λ from 0.01 to 0.1 results in approximately 10% longer computation time, rising from 1.12 seconds to 1.23 seconds per

Table 4: Effect of regularization weight λ on mesh quality. Fixed: $\delta = 0.5$, 53 meshes, 1000 iterations, 10000 sampled points.

λ	**HD** $\downarrow$	**NC** $\uparrow$	**Time/mesh (s)**
0.001	0.0367	0.917	**1.12**
0.01	**0.0365**	**0.918**	1.22
0.1	0.037	0.915	1.23

mesh. In terms of Normal Consistency, performance slightly decreases as we increment λ, dropping from 0.918 at lower values to 0.915 at $\lambda = 0.1$. These results suggest that lower regularization weights provide the best balance between quality and computational efficiency.

Table 5: Effect of edge constraint threshold δ on mesh quality. Fixed: $\lambda = 0.1$, 53 meshes, 1000 iterations, 10000 sampled points.

δ	**HD** $\downarrow$	**NC** $\uparrow$	**Time/mesh (s)**
0.005	0.330	0.688	4.74
0.05	0.075	0.894	1.58
0.5	**0.038**	**0.917**	**1.22**

As evidenced in Table 5, reducing δ from the default value of 0.5 substantially degrades generation quality while increasing computational overhead. At $\delta = 0.005$, the Hausdorff Distance increases nearly 9-fold, while Normal Consistency has a 25% decrease compared to the default setting. Computational time increases by up to 3.9× as the algorithm relaxes smoothness constraints that force alignment of adjacent edges. Even the intermediate setting of $\delta = 0.05$ shows degraded performance on Hausdorff and normal consistency metrics. Also, it takes 28% more computation time to complete the task because the solver isn't able to achieve a proper solution on less steps, requiring more iterations to do it.

Between the two hyperparameters we can see that δ has much more impact on the entire process, what confirms that the smoothness constraint is highly important for the conic solver to return an accurate representation.

6.1 Limitations

We found that some of the meshes have elements that were not properly optimized and exhibited surface artifacts. In Figure 6, it can be observed

how the upper part of a kitchen, where all the control knobs are located, displays geometric irregularities between these elements.

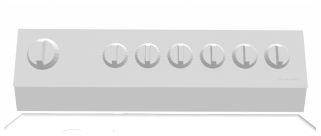

Figure 6: Failure case of MeshCone on a specific mesh from a kitchen

While the convex optimization framework provides strong theoretical guarantees, it occasionally struggles with preserving extremely high-frequency details in complex geometric regions. The global nature of our centroid-alignment objective and edge-length constraints can over-smooth localized details. These limitations could be addressed in future work through localized optimization that decomposes the mesh into regions with independent convex subproblems, or multi-scale refinement strategies that apply hierarchical optimization at different resolution levels.

In addition, we find that highly detailed meshes are inherently difficult to represent perfectly due to the large discrepancy in the number of faces between the ground-truth meshes and the generated ones, such as those from the dataset used in [5].

7 Future Work

While this work establishes what pure convex optimization can achieve for mesh improvement, we envision significant potential in hybrid architectures that combine the mathematical guarantees of our method with the expressive power of deep learning. One promising direction is to use learned priors to guide the optimization process: neural networks could predict optimal hyperparameters λ and δ conditioned on input geometry, or learn to initialize vertex positions in regions where the convex formulation struggles.

A more ambitious future is to combine our method with mesh generators like diffusion models or auto-regressive models. The AI would create rough mesh shapes, and our optimization would automatically refine them into smooth, geometrically correct meshes. This should be an interesting solution for artists that could generate better representations by combining the best of the two worlds.

8 Conclusions

This work introduced MeshCone, a convex optimization framework for geometry-guided mesh refinement that leverages reference geometry to achieve provably optimal corrections. Through this research, we demonstrated that high-quality refinement can be achieved while preserving the intrinsic geometric and topological properties of the input meshes. Our tests on ShapeNet and ThreeDScans confirmed that the framework enhances meshes by improving vertex alignment and edge consistency while enforcing smoothness in the final representation. MeshCone enables users to refine meshes with minimal hyperparameter tuning and no training requirements, making it suitable for workflows where reference geometry is available, such as template-based modeling, scan-to-CAD alignment, and asset production pipelines.

We believe that the future of geometric deep learning lies not in replacing optimization with learning, but in principled integration of both paradigms. This work provides a rigorous mathematical foundation upon which hybrid methods can be built, offering a path toward systems that combine the expressiveness of generative models with the guarantees of convex optimization.

A Supplementary Materials

A.1 Theoretical Properties

The proposed framework is grounded in conic optimization theory [4,9], providing strong mathematical guarantees for convergence, stability, and global optimality. A general conic optimization problem can be formulated as:

$$\begin{array}{lll} \underset{x,\,s}{\text{minimize}} & \frac{1}{2}x^\top Px + c^\top x & \underset{y}{\text{maximize}} \quad -b^T y \\ \text{subject to} & Ax + s = b, & \text{subject to} \quad -A^T y + r = c, \\ & s \in \mathcal{K}. & \qquad\qquad (r, y) \in \{0\}^n \times \mathcal{K}^*. \end{array} \tag{4}$$

where $\mathcal{K}$ denotes a convex cone. Because both the objective and feasible region are convex, every local optimum is also a global optimum, ensuring deterministic and stable convergence without initialization bias. The convexity of both $f(\mathbf{x})$ and $\mathcal{K}$ implies that the feasible set is convex and closed. Hence, the solution $\mathbf{x}^\star$ obtained by the solver corresponds to a global minimum. This property contrasts sharply with non-convex or neural approaches that may converge to suboptimal local minima.

In our conic maximization problem, $b \in \mathbb{R}^m$ and $c \in \mathbb{R}^n$ denote the data vectors, y is the dual variable, and the dual cone of $\mathbb{R}^n \times \mathcal{K}$ is $\{0\}^n \times \mathcal{K}^*$. Since both $\mathcal{K}^*$ and the dual objective $f(\mathbf{y})$ are convex, the optimal solution $\mathbf{y}^\star$ is a global maximizer.

Based on the properties established above, and by invoking Slater's condition [9], the existence of a strictly feasible point guarantees that strong duality holds. Therefore,

$$p^\star = d^\star, \tag{5}$$

where $p^\star$ and $d^\star$ denote the primal and dual optimal values. This equality ensures that optimality can be certified through dual residuals and allows the Lagrange multipliers to be interpreted as geometric regularizers that enforce smoothness or curvature consistency.

Under non-degeneracy assumptions and strict complementarity [6,45] the conic programs are known to satisfy Lipschitz continuity of the solution mapping with respect to perturbations in $(\mathbf{A}, \mathbf{b}, \mathbf{c})$. Small perturbations in vertex positions or sampling noise lead to bounded changes in the optimal solution:

$$\|\mathbf{x}^\star(\delta) - \mathbf{x}^\star\|_2 \leq L\|\delta\|_2, \quad L > 0, \tag{6}$$

providing robustness to geometric noise and guaranteeing stable mesh refinement.

A.1.1 Smoothness Constraints

In MeshCone, local smoothness is enforced via second-order cone (SOC) constraints of the form:

$$\|\mathbf{L}\mathbf{x}\|_2 \leq \delta, \tag{7}$$

where $\mathbf{L}$ encodes an edge-difference operator [7, 19]. This formulation bounds curvature variation and ensures piecewise-smooth surface reconstruction while maintaining geometric fidelity to the target mesh.

A.1.2 Convergence of Splitting Conic Solvers

The optimization is solved using Splitting Conic Solver (SCS) [42], which employs a primal–dual operator-splitting scheme based on the homogeneous self-dual embedding of the problem. SCS guarantees global convergence:

$$(\mathbf{x}^k, \mathbf{y}^k) \to (\mathbf{x}^\star, \mathbf{y}^\star), \tag{8}$$

with an ergodic rate of $\mathcal{O}(1/k)$ [40, 42] in objective and feasibility residuals. Its efficiency benefits from the sparsity of the constraint matrix $\mathbf{A}$.

The second-order conic programs, have a theoretical complexity per iteration of $\mathcal{O}(n)$ for sparse systems [42], this mean that even when the number of constraints increased, the formulation of $\mathbf{A}$ makes it suitable to perform these computations.

Sparsity Structure of A The constraint matrix $\mathbf{A}$ exhibits natural sparsity arising from the local connectivity of the mesh topology. Each vertex in the input mesh is typically connected to a small, bounded neighborhood, ensuring that each row of $\mathbf{A}$ contains only $\mathcal{O}(1)$ non-zero entries. Additionally, the discrete differential operator $\mathbf{L}$ encodes only pairwise differences between adjacent vertices, yielding a sparse banded structure with $\text{nnz}(\mathbf{A}) = \mathcal{O}(n)$, where n is the number of vertices.

This sparsity pattern ensures that even as the number of constraints grows proportionally with the number of edges $|E| = \mathcal{O}(n)$ (for bounded-degree meshes), the computational cost per iteration remains linear: $\mathcal{O}(\text{nnz}(\mathbf{A})) = \mathcal{O}(n)$. Consequently, MeshCone scales efficiently with mesh resolution without sacrificing geometric fidelity.

A.2 Solver Structure and Problem Dimensions

In 6 we included the configuration and structure of a Splitting Conic Solver optimization problem based on one of our meshes. The problem is made from 40,169 variables and 68,128 constraints, which makes it ideal for this type of optimizer that focuses on large problems.

Table 6: SCS problem structure for a representative mesh.

Problem Size	
Variables (n)	40,169
Constraints (m)	68,128
Cone Structure	
Primal zero / dual free vars (z)	20,418
Linear vars (l)	9,542
SOC vars (q)	38,168
SOC block size	9,542
Solver Settings	
Absolute tolerance	1×10^{-5}
Relative tolerance	1×10^{-5}
Infeasibility tolerance	1×10^{-7}
Max iterations	1000
Alpha (relaxation)	1.50
Scaling	1.0×10^{-1}
Adaptive scaling	Yes
Normalization	Yes
ρ_x	10^{-6}
Acceleration lookback	10
Acceleration interval	10
Linear System Solver	
Type	sparse-direct-amd-qdldl
nnz(A)	117,172
nnz(P)	20,418

The Cone Structure part indicates the variables with no constraints in the primal formulation, which are 20,418, and the ones with linear constraints, which are 9,542. The SOC vars represent the variables subject to Second-Order Cone constraints (quadratic cone constraints of the form $\|x\| \leq t$), totaling 38,168 variables organized into 4 blocks of 9,542 variables each.

The nnz(A) and nnz(P) are the respective constraint matrix and cost matrix. It is important to notice that given the sparsity of P (with only 20,418 non-zero entries compared to 117,172 in A), we can achieve faster convergence on the dual residual due to the efficiency of sparse matrix operations. The cost matrix P being approximately 5.7 times sparser than the constraint matrix A enables more efficient computation of dual updates in the ADMM algorithm.

Table 7: SCS convergence diagnostics for a representative mesh. Values shown for the first iteration and the iteration at convergence (iteration 25).

Iter	Pri. res.	Dual res.	Gap	Obj.	Scale	Time (s)
0	5.00×10^{-1}	3.47×10^{-3}	1.51×10^{1}	7.55	1.0×10^{-1}	6.25×10^{-2}
25	1.00×10^{-8}	8.61×10^{-12}	1.51×10^{-7}	3.77	1.0×10^{-1}	1.05×10^{-1}

We can see in 7 that the solver achieves an optimal solution at its 25th iteration approximately, where the primal residual (Pri. res) reaches a value lower than the absolute tolerance indicated in 6. The dual residual (Dual res) also converges below the specified tolerance at approximately the same iteration. The convergence behavior shows a smooth monotonic decrease in both residuals, which is typical for conic optimization problems. Additionally, the gap between the primal and dual objective values decreases steadily, confirming that the solution approaches optimality.

References

[1] Frédéric Alauzet and Adrien Loseille. High-order sonic boom modeling based on adaptive methods. *Journal of Computational Physics*, 229(3):561–593, 2010.

[2] Nina Amenta, Marshall Bern, and David Eppstein. Surface reconstruction by voronoi filtering. In *Discrete & Computational Geometry*, volume 22, pages 481–504. Springer, 1999.

[3] Ivo Babuška and Werner C. Rheinboldt. Error estimates for adaptive finite element computations. *SIAM Journal on Numerical Analysis*, 15(4):736–754, 1978. Foundational work establishing a posteriori error estimation for adaptive FEM.

[4] Aharon Ben-Tal and Arkadi Nemirovski. *Lectures on modern convex optimization: analysis, algorithms, and engineering applications*. SIAM, 2001.

[5] Alexandre Binninger, Ruben Wiersma, Philipp Herholz, and Olga Sorkine-Hornung. Tetweave: Isosurface extraction using on-the-fly delaunay tetrahedral grids for gradient-based mesh optimization. *ACM Transactions on Graphics*, 44(4):1–19, July 2025.

[6] J Frédéric Bonnans and Alexander Shapiro. Perturbation analysis of optimization problems. *Springer Series in Operations Research*, 1998.

[7] Mario Botsch, Leif Kobbelt, Mark Pauly, Pierre Alliez, and Bruno Lévy. Polygon mesh processing. 2010.

[8] Stephen Boyd, Neal Parikh, Eric Chu, Borja Peleato, and Jonathan Eckstein. Distributed optimization and statistical learning via the alternating direction method of multipliers. *Foundations and Trends in Machine Learning*, 3(1):1–122, 2011.

[9] Stephen Boyd and Lieven Vandenberghe. *Convex Optimization*. Cambridge University Press, 2004.

[10] Carsten Burstedde, Lucas C. Wilcox, and Omar Ghattas. p4est: Scalable algorithms for parallel adaptive mesh refinement on forests of octrees. *SIAM Journal on Scientific Computing*, 33(3):1103–1133, 2011.

[11] Angel X. Chang, Thomas Funkhouser, Leonidas Guibas, Pat Hanrahan, Qixing Huang, Zimo Li, Silvio Savarese, Manolis Savva, Shuran Song, Hao Su, Jianxiong Xiao, Li Yi, and Fisher Yu. Shapenet: An information-rich 3d model repository, 2015.

[12] Wenzheng Chen, Jun Gao, Huan Ling, Edward J. Smith, Jaakko Lehtinen, Alec Jacobson, and Sanja Fidler. Learning to predict 3d objects with an interpolation-based differentiable renderer (dib-r). In *Advances in Neural Information Processing Systems (NeurIPS)*, 2019.

[13] Yiwen Chen, Tong He, Di Huang, Weicai Ye, and Sanja Fidler. Meshanything: Artist-created mesh generation with autoregressive transformers. *arXiv preprint arXiv:2406.10163*, 2024.

[14] Yiwen Chen, Tong He, Di Huang, Weicai Ye, and Sanja Fidler. Meshanything v2: Artist-created mesh generation with adjacent mesh tokenization. In *ICCV*, 2025.

[15] Zhiqin Chen and Hao Zhang. Neural marching cubes. *ACM Transactions on Graphics*, 40(6):1–15, December 2021.

[16] Philippe G. Ciarlet. *The Finite Element Method for Elliptic Problems*. SIAM, Philadelphia, PA, 2002.

[17] Brian Curless and Marc Levoy. A volumetric method for building complex models from range images. *Proceedings of SIGGRAPH*, pages 303–312, 1996.

[18] Bailin Deng, Kyle Genova, Soroosh Yazdani, Sofien Bouaziz, Paul Guerrero, Sanja Fidler, and Thomas Funkhouser. Cvxnet: Learnable convex decomposition. In *Proceedings of the IEEE/CVF Conference on Computer Vision and Pattern Recognition (CVPR)*, pages 31–41, 2020.

[19] Mathieu Desbrun, Mark Meyer, Peter Schröder, and Alan H Barr. Implicit fairing of irregular meshes using diffusion and curvature flow. *SIGGRAPH*, pages 317–324, 1999.

[20] Lori A. Freitag and Carl Ollivier-Gooch. Tetrahedral mesh improvement using swapping and smoothing. *International Journal for Numerical Methods in Engineering*, 40(21):3979–4002, 1997.

[21] Pascal J. Frey and Frédéric Alauzet. Anisotropic mesh adaptation for cfd computations. *Computer Methods in Applied Mechanics and Engineering*, 194(48-49):5068–5082, 2005.

[22] Jun Gao, Xuejian Song, Mingyuan Yin, Edward J. Smith, and Sanja Fidler. Get3d: A generative model of high quality 3d textured shapes learned from images. In *Advances in Neural Information Processing Systems (NeurIPS)*, 2022.

[23] Georgia Gkioxari, Jitendra Malik, and Justin Johnson. Mesh r-cnn. In *Proceedings of the IEEE/CVF International Conference on Computer Vision (ICCV)*, 2019.

[24] Thibault Groueix, Matthew Fisher, Vladimir G. Kim, Bryan C. Russell, and Mathieu Aubry. Atlasnet: A papier-mâché approach to learning 3d surface generation. In *Proceedings of the IEEE Conference on Computer Vision and Pattern Recognition (CVPR)*, 2018.

[25] David Held, Anant Dahiya, and Sanja Fidler. 3d convex splatting for radiance field rendering. *arXiv preprint arXiv:2402.12345*, 2024.

[26] Jiahui Huang, Yifan Wang, Shihao Wu, Hsueh-Tien Liu, Danny M. Kaufman, and Justin Solomon. Quadriflow: A scalable and robust method for quadrangulation. In *Proceedings of the IEEE/CVF Conference on Computer Vision and Pattern Recognition (CVPR)*, pages 4350–4358, 2018.

[27] Wenzel Jakob, Marco Tarini, Daniele Panozzo, and Olga Sorkine-Hornung. Instant field-aligned meshes. *ACM Transactions on Graphics (TOG)*, 34(6):189:1–189:15, 2015.

[28] Hiroharu Kato, Yoshitaka Ushiku, and Tatsuya Harada. Neural 3d mesh renderer. In *Proceedings of the IEEE Conference on Computer Vision and Pattern Recognition (CVPR)*, 2018.

[29] Michael Kazhdan, Matt Bolitho, and Hugues Hoppe. Poisson surface reconstruction. *Proceedings of the Fourth Eurographics Symposium on Geometry Processing*, pages 61–70, 2006.

[30] Bernhard Kerbl, Georgios Kopanas, Thomas Leimkühler, and George Drettakis. 3d gaussian splatting for real-time radiance field rendering. In *ACM SIGGRAPH 2023 Conference Proceedings*, 2023.

[31] Bryan Matthew Klingner and Jonathan Richard Shewchuk. Aggressive tetrahedral mesh improvement. *Proceedings of the 16th International Meshing Roundtable*, pages 3–23, 2007.

[32] Olivier Laric. Three d scans: Free downloadable 3d scans. https://threedscans.com/, 2012. Scans based on collections from Albertina, Vienna; Kunsthistorisches Museum, Vienna; Musée Guimet, Paris; and other institutions. Supported by Lafayette Anticipation, Secession, and others. No copyright restrictions. Accessed: 2024-12-08.

[33] Zhenwei Lin, Zikai Xiong, Dongdong Ge, and Yinyu Ye. Pdcs: A primal-dual large-scale conic programming solver with gpu enhancements, 2025.

[34] Samuel Lionar, Jiahui Liang, Yiwen Chen, Weicai Ye, and Sanja Fidler. Treemeshgpt: Artistic mesh generation with autoregressive tree sequencing. In *Proceedings of the IEEE/CVF Conference on Computer Vision and Pattern Recognition (CVPR)*, 2025.

[35] William E. Lorensen and Harvey E. Cline. Marching cubes: A high resolution 3d surface construction algorithm. *SIGGRAPH Comput. Graph.*, 21(4):163–169, August 1987.

[36] William E. Lorensen and Harvey E. Cline. Marching cubes: A high resolution 3d surface construction algorithm. In *Proceedings of the 14th Annual Conference on Computer Graphics and Interactive Techniques (SIGGRAPH)*, pages 163–169, 1987.

[37] Adrien Loseille and Frédéric Alauzet. Continuous mesh framework part i: Well-posed continuous interpolation error. *SIAM Journal on Numerical Analysis*, 49(1):38–60, 2011.

[38] Peter MacNeice, Kevin M. Olson, Clark Mobarry, Rosalinda de Fainchtein, and Charles Packer. Paramesh: A parallel adaptive mesh refinement community toolkit. *Computer Physics Communications*, 126(3):330–354, 2000.

[39] Charlie Nash, Yaroslav Ganin, S. M. Ali Eslami, and Peter Battaglia. Polygen: An autoregressive generative model of 3d meshes. In *Proceedings of the 37th International Conference on Machine Learning (ICML)*, pages 7223–7233, 2020.

[40] Yurii Nesterov. Smooth minimization of non-smooth functions. *Mathematical programming*, 103(1):127–152, 2005.

[41] Brendan O'Donoghue, Eric Chu, Neal Parikh, and Stephen Boyd. Conic optimization via operator splitting and homogeneous self-dual embedding. *Journal of Optimization Theory and Applications*, 169(3):1042–1068, June 2016.

[42] Brendan O'Donoghue, Eric Chu, Neal Parikh, and Stephen Boyd. Conic optimization via operator splitting and homogeneous self-dual embedding. *Journal of Optimization Theory and Applications*, 169:1042–1068, 2016.

[43] Maria-Cecilia Rivara. Mesh refinement processes based on the generalized bisection of simplices. *SIAM Journal on Numerical Analysis*, 21(3):604–613, 1984.

[44] Maria-Cecilia Rivara. New longest-edge algorithms for the refinement and/or improvement of unstructured triangulations. *International Journal for Numerical Methods in Engineering*, 40(18):3313–3324, 1997.

[45] Stephen M Robinson. Strongly regular generalized equations. *Mathematics of operations research*, 5(1):43–62, 1980.

[46] Robert Schneiders, Ralf Schindler, and Franz Weiler. Octree-based generation of hexahedral element meshes. In *Proceedings of the 5th International Meshing Roundtable*, pages 205–215, 1996.

[47] Tianchang Shen, Jun Gao, Kangxue Yin, Ming-Yu Liu, and Sanja Fidler. Deep marching tetrahedra: a hybrid representation for high-resolution 3d shape synthesis. In *Advances in Neural Information Processing Systems (NeurIPS)*, volume 34, pages 6087–6101, 2021.

[48] Tianchang Shen, Jacob Munkberg, Jon Hasselgren, Kangxue Yin, Zian Wang, Wenzheng Chen, Zan Gojcic, Sanja Fidler, Nicholas Sharp, and Jun Gao. Flexible isosurface extraction for gradient-based mesh optimization. In *ACM SIGGRAPH 2023 Conference Proceedings*, pages 1–10, 2023.

[49] Weili Sheng, Zhixun Su, and Junjun Zhang. Efficient large-scale texture mapping using mesh-based continuous max-flow. *Computer-Aided Design*, 136:143, 2021.

[50] Jonathan Richard Shewchuk. What is a good linear finite element? interpolation, conditioning, anisotropy, and quality measures. *Proceedings of the 11th International Meshing Roundtable*, pages 115–126, 2002.

[51] Jonathan Richard Shewchuk. What is a good linear finite element? interpolation, conditioning, anisotropy, and quality measures. In *Proceedings of the 11th International Meshing Roundtable*, pages 115–126. Springer, 2002.

[52] Yawar Siddiqui, Antonio Alliegro, Alexey Artemov, Tatiana Tommasi, and Matthias Nießner. Meshgpt: Generating triangle meshes with decoder-only transformers. In *Proceedings of the IEEE/CVF Conference on Computer Vision and Pattern Recognition (CVPR)*, 2024.

[53] Edward J. Smith, Chen Fang, Weiyu Liu, Xiaogang Zhang, Spencer Hill, and Sanja Fidler. Geometrics: Exploiting geometric structure for graph-encoded objects. In *Proceedings of the International Conference on Machine Learning (ICML)*, 2019.

[54] Hari Sundar, Rahul S. Sampath, and George Biros. Bottom-up construction and 2:1 balance refinement of linear octrees in parallel. *SIAM Journal on Scientific Computing*, 30(5):2675–2708, 2008.

[55] Jie Tang, Weiyu Li, Yiwen Chen, and Sanja Fidler. Arae: An autoregressive auto-encoder for artistic mesh generation. *arXiv preprint arXiv:2409.18114*, 2024.

[56] Rüdiger Verfürth. *A Review of A Posteriori Error Estimation and Adaptive Mesh-Refinement Techniques*. John Wiley & Sons, Chichester, UK, 1996.

[57] Nanyang Wang, Yinda Zhang, Zhuwen Li, Yanwei Fu, Wei Liu, and Yu-Gang Jiang. Pixel2mesh: Generating 3d mesh models from single rgb

images. In *Proceedings of the European Conference on Computer Vision (ECCV)*, 2018.

[58] Tianyu Wang, Bowen Zhang, Yizhou Liu, and Sanja Fidler. Meshmamba: Multi-resolution mesh generation with state space models. In *CVPR*, 2025.

[59] Chao Wen, Yinda Han, Kaichun Wang, and Yizhou Yu Liu. Pixel2mesh++: Multi-view 3d mesh generation via deformation. In *Proceedings of the IEEE/CVF International Conference on Computer Vision (ICCV)*, 2019.

[60] Bowen Zhang, Weiyu Li, Tong He, Di Huang, Weicai Ye, et al. Meshart: Artistic 3d mesh generation with autoregressive transformers. In *NeurIPS*, 2024.

[61] Yongjie Zhang and Chandrajit Bajaj. Adaptive and quality quadrilateral/hexahedral meshing from volumetric data. *Computer Methods in Applied Mechanics and Engineering*, 195(9-12):942–960, 2006.

[62] Hongkai Zhao, Stanley Osher, and Ronald Fedkiw. Fast surface reconstruction using the level set method. *Proceedings of the IEEE Workshop on Variational and Level Set Methods*, pages 194–202, 2001.